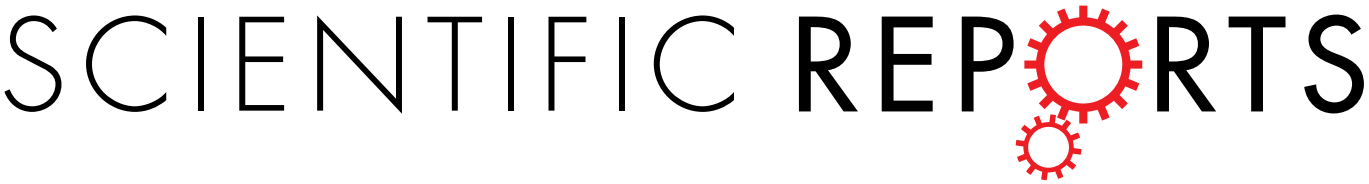

OPEN

Innovatively Continuous Mass Production Couette-taylor Flow: Pure Inorganic Green-Emitting Cs_4PbBr_6 Perovskite Microcrystal for display technology

Received: 2 October 2017
Accepted: 17 January 2018
Published online: 31 January 2018

Young Hyun Song[1], Seung Hee Choi[2], Won Kyu Park[2], Jin Sun Yoo[3], Seok Bin Kwon[2], Bong Kyun Kang[2], Sang Ryul Park[1], Young Soo Seo[1], Woo Seok Yang[3] & Dae Ho Yoon[2]

We report for the first time the mass production of Cs_4PbBr_6 perovskite microcrystal with a Couette-Taylor flow reactor in order to enhance the efficiency of the synthesis reaction. We obtained a pure Cs_4PbBr_6 perovskite solid within 3 hrs that then realized a high photoluminescence quantum yield (PLQY) of 46%. Furthermore, the Cs_4PbBr_6 perovskite microcrystal is applied with red emitting K_2SiF_6 phosphor on a blue-emitting InGaN chip, achieving a high-performance luminescence characteristics of 9.79 lm/W, external quantum efficiency (EQE) of 2.9%, and correlated color temperature (CCT) of 2976 K; therefore, this perovskite is expected to be a promising candidate material for applications in optoelectronic devices.

Due to their remarkable photoelectric properties, cesium lead halide perovskites ($CsPbX_3$) have recently been widely developed for applications in optoelectronic devices such as displays, light emitting diodes (LED)[1,2], solar cells[3,4], photodetectors[5] and lasers[6,7].

In particular, the rapid advances in perovskite materials have drawn significant attention to quantum dots (QD) based on the perovskite for use in light-emitting diodes as replacements of conventional QDs such as CdSe/ZnS QDs[8,9]. The QDs based on the $CsPbX_3$ perovskite materials were synthesized with the hot injection method and showed narrow emission, high photoluminescence quantum yields over 90%, wide wavelength tunability (400–800 nm) and wide color gamut, thus meeting the requirements of display technology[1,10–12]. Although this optical performance is impressive, there are still challenges that must be overcome for practical use of $CsPbX_3$ QDs, such as the realization of large-scale fabrication[13,14] and stability in moisture when exposed to ambient conditions[15–17]. Therefore, several strategies for not only realization of a high photoluminescence quantum yield (PLQY) but also obtaining stability, such as alloying, passivation, and use of polymer/QD composites have been reported[16–20].

An alternative fascinating approach to achieve the high PLQY with quantum confinement is to reduce the structural dimensionality of the perovskite[21–23]. The general formula of the perovskite structure is A_nBX_{2+n}, where A is a monovalent cation, B is a divalent metal, and X is a halogen anion. As the n value increases from 1 to 4, the dimensionality of the perovskite structure changes from 3D, to 2D, 1D and 0D, respectively[24,25]. Recently, many studies have reported a remarkable enhancement of PLQY with the change of perovskite dimensionality[26–28]. In the case of the Cs_4PbBr_6 solid with the 0D octahedron structure, the PLQY was reported to be 45% higher than that of the 3D structure[28].

[1]Department of Nanotechnology and Advanced Material Engineering, Sejong University, 209 Neungdong-ro, Gwangjin-gu, Seoul, 05006, Republic of Korea. [2]School of Advanced Materials Science and Engineering, Sungkyunkwan University, Suwon, 440–746, Republic of Korea. [3]Electronic Materials and Device Research Center, Korea Electronics Technology Institute, Seongnam, 463–816, Republic of Korea. Young Hyun Song, Seung Hee Choi and Won Kyu Park contributed equally to this work. Correspondence and requests for materials should be addressed to W.S.Y. (email: wsyang@keti.re.kr) or D.H.Y. (email: dhyoon@skku.edu)

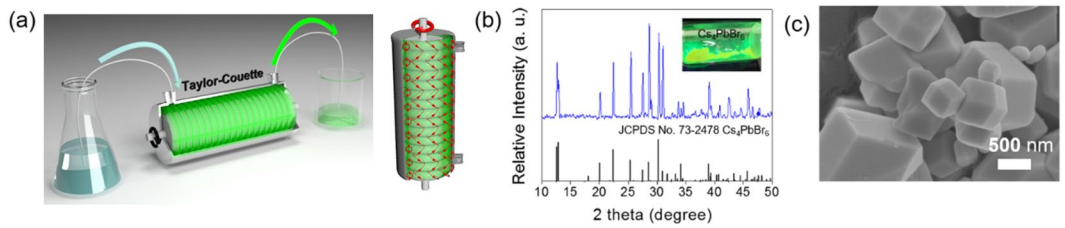

Figure 1. (**a**) Scheme of Synthesis and (**b**) PXRD Patterns (**c**) SEM Image of Cs_4PbBr_6 Perovskite Material.

In the LED packaging process, solid state powder is generally more convenient to apply to optoelectronic applications as well as LED package relative to the film form. It is more useful if a fully inorganic Cs_4PbBr_6 perovskite solid can be produced on a large scale. Although the synthesis and optical characteristics of Cs_4PbBr_6 solid have been reported, to the best of our knowledge, there has been no report on the large-scale production of the Cs_4PbBr_6 solid.

Herein, we report for the first time the large-scale synthesis of green-emitting Cs_4PbBr_6 perovskite solid as a promising candidate for application in optoelectronic devices via the Couette-Taylor flow method. To date, only mass production of graphene oxide (GO) has been reported within the framework of the Couette-Taylor flow method. The Couette-Taylor flow reactor consists of two coaxial cylinders with inner cylinder rotating and generating toroidal vortices that are regularly spaced along the cylinder axis at the critical rotating speed. This toroidal motion of fluids leads to a highly efficient radial mixing of reactant in the system, thereby enhancing the synthesis reaction efficiency. Fully inorganic Cs_4PbBr_6 perovskite powder were used as the luminescence source in the electroluminescence of LEDs. The optimized contents of Cs_4PbBr_6 perovskite powder displayed an outstanding PLQY as well as 1931 CIE coordinates for device performance. This technique can be an important method for application in the fabrication of optoelectronic devices.

Materials and Synthesis

To prepare the Cs_4PbBr_6 perovskite powder, all chemicals were used without purification: cesium bromide (CsBr, 99.99%) lead (II) bromide ($PbBr_2$, 98%), oleic acid (OA, 65.0–88.0%), oleylamine (OAm, 70%), dimethylformamide (DMF, 99%), hexane (n-hex, 90%), cyclohexane (cyclo-hex, 90%) and toluene (Tol, 99%) were acquired from Sigma Aldrich.

For synthesis of the Cs_4PbBr_6 perovskite microcrystals with the Couette-Taylor flow method, 42.562 g of CsBr (0.2 mol) and 73.402 g of $PbBr_2$ (0.2 mol) precursor were dissolved in 5 L of DMF. Then, prepared 500 mL of OA and 500 mL OLA were added to 5 L of an n-hexane medium reactor solution. Precursor and medium reactor solutions were added in the Couette-Taylor flow reactor by a peristaltic pump at the same time and same volume (20 mL/min). The Couette-Taylor flow reactor (length: 500 mm) consists of two coaxial cylinders: the outer cylinder (radius: 68 mm) is fixed, and the inner cylinder (radius: 60 mm) rotates. After each solution was introduced into the gap between the two cylinders, the inner cylinder was rotated. The rotating speed of the inner cylinder was 1000 rpm for the reaction time. The mixture in a Couette-Taylor flow reactor produced a green-colored reactant within 15 min. To examine the dependence of the luminous characteristics on the synthetic technique, the stirring method is introduced. 0.085 g of CsBr (0.4 mmol) and 0.146 g of $PbBr_2$ (0.4 mmol) were dissolved in 10 mL of DMF. After dissolving the precursor solution, 10 mL was quickly injected into the medium reactor solution, consisting of OA (1 mL) and OAm (1 mL) in 10 mL of n-hexane to induce the reaction via various stirring conditions. The solution color was changed from milky-white to yellow-green. Then, after continuous stirring for 30 minutes, strong green emission was observed under a 365-nm wavelength lamp. The solutions were separated by centrifugation at 4000 rpm for 5 minutes. Then, the supernatant was discarded, and the collected precipitant was washed with 10 mL of cyclohexane. Finally, the precipitant was dried with a freeze-drier to obtain the Cs_4PbBr_6 powder. All processes were carried out at room temperature.

Characterization. The crystalline phase of the Cs_4PbBr_6 perovskite was identified using X-ray diffraction (XRD, D-MAX 2500, Rigaku, Tokyo, Japan) with Ni-filtered Cu Kα radiation. The XRD pattern was recorded in the 2θ range of 10°–50°. The photoluminescence (PL) were examined using a spectrometer (SCINCO, FS-2, Korea) in the range of 400–700 nm with a xenon lamp excitation source (150 W). The microstructure and morphology of the samples was investigated using field emission scanning electron microscopy (FE-SEM, JSM-7000F, JEOL). The absolute quantum yield (absQY) was measured using the absolute PL quantum yield measurement system of Hamamatsu C9920–2 and the PL intensity, luminous efficacy, CRI, CCT, CIE coordinate number of the LED operating at 3.2 V and 20, 40, 60, 70 mA were measured using the CSLMS LED 1060 of Labsphere.

Results

Figure 1(a) shows the procedure for the synthesis of green-emitting Cs_4PbBr_6 perovskite materials. PXRD patterns of the green-emitting Cs_4PbBr_6 prepared via the Couette-Taylor flow method were obtained. The prepared Cs_4PbBr_6 sample shows good agreement with the JCPDS reference No. 73–2478, and no impurity phase is detected; the sample has a crystal structure with a rhombohedral crystal system and lattice parameters of a = b = 13.73 Å and c = 17.31 Å as shown in Fig. 1(b). By using the Couette-Taylor flow method, we confirm the possibility of synthesis of the various perovskite materials such as $CsPbBr_3$, Cs_2PbBr_4, and Cs_4PbBr_6 for innovative mass production. To examine the morphology of the synthesized materials, a field-emission scanning electron microscopy (FE-SEM) image of the synthesized microcrystal using the Couette-Tayler flow method was obtained

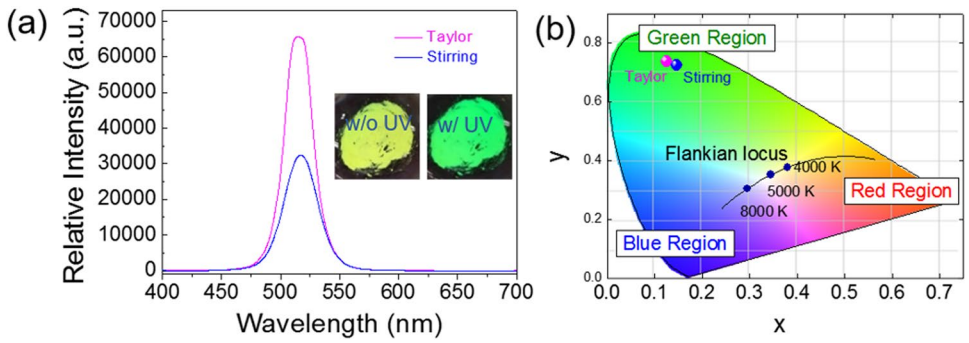

Figure 2. (**a**) Photoluminescence Properties and (**b**) CIE Color Space of Cs_4PbBr_6 Perovskite Material.

Sample	CIE coordinate		FWHM (nm)	PLQY (%)
	X	Y		
Taylor method	0.125	0.737	26.63	46
Stirring method	0.147	0.724	33.2	35

Table 1. Overall Luminous Characteristics with Synthetic Technique.

Composition ratio KSF: Perov. (wt%)	Luminous Efficacy (lm/W)	CRI(%)	CCT (K)	CIE coordinate	
				x	y
0.2: 1	7.46	65.345	6563	0.2935	0.4506
0.4: 1	8.87	42.824	4521	0.3623	0.3765
0.6: 1	9.79	34.772	2976	0.4445	0.4165
0.8: 1	7.51	34.577	1777	0.5439	0.3979
20 mA, 2.85 V					

Table 2. Overall Luminous Characteristics for Different Composite Ratios.

and is shown in Fig. 1(c). Formation of rhombic prisms is displayed, which corresponds to Cs_4PbBr_6 perovskite compounds, as well as previous reports.

The photoluminescence (PL) spectra of the Cs_4PbBr_6 perovskite microcrystals are shown in Fig. 2(a) as a function of the synthetic route. The PLQY of approximately 46% in the Cs_4PbBr_6 microcrystal prepared via the Couette-Taylor flow method displayed the higher luminous performance than the 35% for the sample obtained by the stirring method, and a slight variation of 6.57 nm in the full width at half-maximum (FWHM) was observed. This is related to the decrease in the crystalline defects and the improvement of the homogeneity in the Cs_4PbBr_6 microcrystal because the Couette-Taylor flow can intensify the agitation and induce uniform fluidic motion, both of which enhance the uniformity of reactants as well as mass productivity via continuous production. Additionally, the luminous characteristics of the Cs_4PbBr_6 perovskite microcrystal are shown ornation as a function of synthesis temperature in Figure S1 of the supporting Inf. Comprehensively consideration of the color purity for display technology shows that the Cs_4PbBr_6 perovskite microcrystals synthesized using the Couette-Taylor flow method are suitable for use in display applications. The CIE chromaticity coordinates of the Cs_4PbBr_6 perovskite microcrystal is indicated in Fig. 2(b). The CIE color space coordinate of the sample prepared with the Couette Taylor flow method is suited to the green region ($x = 0.1254$, $y = 0.7377$), with high color purity compared to the sample obtained using the stirring method ($x = 0.1473$, $y = 0.7241$). The overall luminous characteristics as a function of synthetic technique are displayed in Table 1.

Electroluminescence properties of a white LED package at the forward-bias current of 20 mA is shown in Fig. 3(a). It consists of a blue-emitting InGaN LED chip, a green-emitting Cs_4PbBr_6 perovskite microcrystal, and a red-emitting K_2SiF_6:Mn^{4+} phosphor for white light generation. To confirm the change of white target, the K_2SiF_6:Mn^{4+} phosphor is composited with Cs_4PbBr_6 perovskite microcrystal with the ratio of 0.2:1, 0.4:1, 0.6:1, and 0.8:1, respectively. The typical electroluminescence (EL) spectrum is obtained, corresponding to the emission wavelength of the Cs_4PbBr_6 perovskite microcrystal and the K_2SiF_6: Mn^{4+} phosphor. Furthermore, luminous efficacy increased with the increasing ratio of the composite. Under the forward-bias current of 20 mA, the highest power efficacies of 9.79 lm W^{-1}, CRI of 34.772, CCT of 2976 K, EQE of 2.9% are observed. With an increasing composite ratio, warm-white light is generated due to the addition of the red component. CIE color space coordinates for practical application in white LED are shown in Fig. 3(b). With an increasing composite ratio, the axis is moved to warm white based on the Flankian locus line, which is suitable for use in lighting technology through a perfect combination of green and red components. Additionally, the National Television System Committee (NTSC) has conducted investigations to identify candidates for next-generation display applications, which encompass 118%.

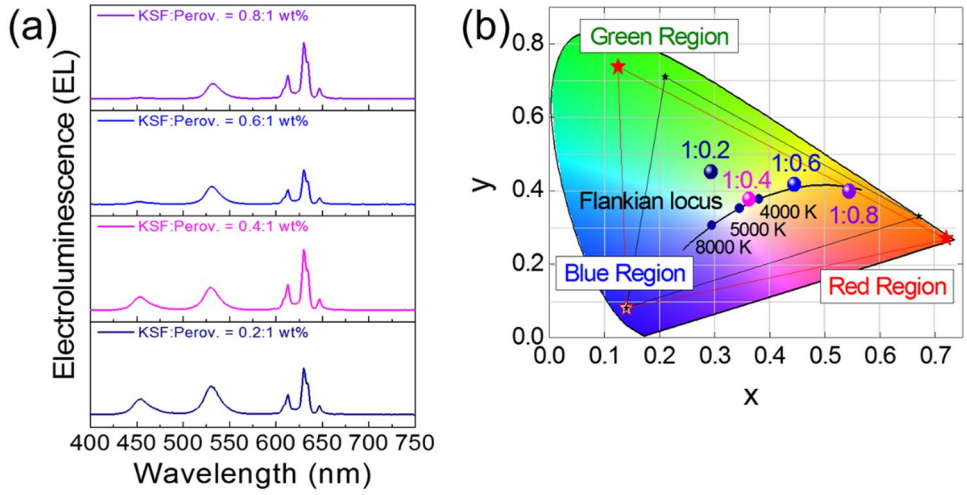

Figure 3. (**a**) Electroluminescence Properties and (**b**) CIE Color Space of Cs_4PbBr_6 Perovskite Material for Different Composite Ratios.

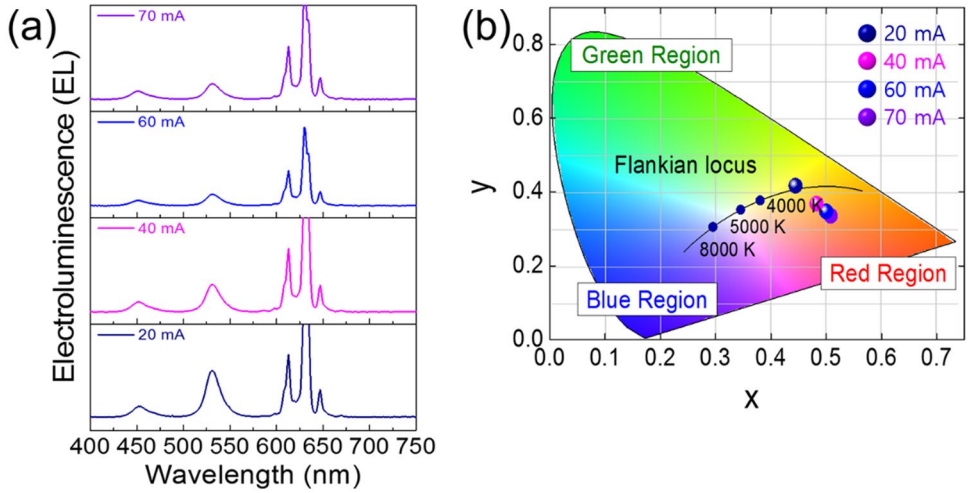

Figure 4. (**a**) Electroluminescence Properties and (**b**) CIE Color Space of Cs_4PbBr_6 Perovskite Material for Different Forward-Current Bias.

Perov.: KSF = 1: 0.6 (wt%)					
Current (mA)	Luminous Efficacy (lm/W)	CRI (%)	CCT (K)	CIE coordinate	
				x	Y
20	9.79	34.772	2976	0.4445	0.4165
40	6.48	30.177	2100	0.4823	0.3681
60	5.08	33.690	1797	0.4999	0.3474
70	4.48	36.642	1657	0.5081	0.3353

Table 3. Overall Luminous Characteristics for Different Forward-Current Bias.

To the best of our knowledge, it is very impressive for Cs_4PbBr_6 perovskite microcrystal to meet the requirements for use in the ultra-high definition (UHD) display. The overall characteristics of the white LED package are presented in Table 2. Based on the composite ratio of 0.6:1 (K_2SiF_6: Cs_4PbBr_6), EL spectra and CIE color space coordinates are analyzed as shown in Fig. 4(a,b). We know that perovskite materials are unstable at higher temperatures. With increasing forward-bias current, the luminous efficacy is decreased from 9.79 to 4.48 lm W^{-1}, and CCT is changed from 2976 to 1657 K due to the unstable characteristics of the Cs_4PbBr_6 perovskite microcrystal. The overall characteristics of the white LED package with the different forward-current bias values are presented in Table 3. Figures S2, S3, and S4 of the Supporting Information show the CIE color space coordinates as a function of the composite ratio under different forward-bias currents of 20, 40, 60 and 70 mA.

Conclusion

In summary, we have developed an innovative synthetic technique of Cs_4PbBr_6 perovskite microcrystal using Couette taylor flow method. The prepared Cs_4PbBr_6 perovskite microcrystal shows the behavior of excellent luminous properties with narrow FWHM and mass production possibility. Through these results, we believe that our innovative technique will represent a new strategy for applications in optoelectronic device, and findings are new family member as a next generation candidate in field of luminescence materials[29,30].

References

1. Protesescu, L. *et al*. Nanocrystals of cesium lead halide perovskites ($CsPbX_3$, X = Cl, Br, and I): novel optoelectronic materials showing bright emission with wide color gamut. *Nano Lett.* **15**, 3692–3696 (2015).
2. Song, J. *et al*. Quantum dot light-emitting diodes based on inorganic perovskite cesium lead halides ($CsPbX_3$). *Adv. Mater.* **27**, 7162–7167 (2015).
3. Kulbak, M., Cahen, D. & Hodes, G. How important is the organic part of lead halide perovskite photovoltaic cells? efficient $CsPbBr_3$ cells. *J. Phys. Chem. Lett.* **6**, 2452–2456 (2015).
4. Eperon, G. E. *et al*. Inorganic caesium lead iodide perovskite solar cells. *J. Mater. Chem. A* **3**, 19688–19695 (2015).
5. Liu, X. *et al*. Low-voltage photodetectors with high responsivity based on solution-processed micrometer-scale all-inorganic perovskite nanoplates. *Small* **13**, 1700364 (2017).
6. Yakunin, S. *et al*. Low-threshold amplified spontaneous emission and lasing from colloidal nanocrystals of caesium lead halide perovskites. *Nat. Commun.* **6**, 8056 (2015).
7. Wang, Y. *et al*. All-inorganic colloidal perovskite quantum dots: a new class of lasing materials with favorable characteristics. *Adv. Mater.* **27**, 7101–7108 (2015).
8. Swarnkar, A. *et al*. Colloidal $CsPbBr_3$ perovskite nanocrystals: luminescence beyond traditional quantum dots. *Angew. Chem.* **127**, 15644–15648 (2015).
9. Veldhuis, S. A. *et al*. Perovskite materials for light-emitting diodes and lasers. *Adv. Mater.* **28**, 6804–6834 (2016).
10. Nedelcu, G. *et al*. Fast anion-exchange in highly luminescent nanocrystals of cesium lead halide perovskites ($CsPbX_3$, X = Cl, Br, I). *Nano Lett.* **15**, 5635–5640 (2015).
11. Bai, S., Yuan, Z. & Gao, F. Colloidal metal halide perovskite nanocrystals: synthesis, characterization, and applications. *J. Mater. Chem. C* **4**, 3898–3904 (2016).
12. Bai, Z. & Zhong, H. Halide perovskite quantum dots: potential candidates for display technology. *Sci. Bull.* **60**, 1622–1624 (2015).
13. Wei, S. *et al*. Room-temperature and gram-scale synthesis of $CsPbX_3$ (X = Cl, Br, I) perovskite nanocrystals with 50–85% photoluminescence quantum yields. *Chem. Commun.* **52**, 7265–7268 (2016).
14. Chen, X. *et al*. Non-injection gram-scale synthesis of cesium lead halide perovskite quantum dots with controllable size and composition. *Nano Res.* **9**, 1994–2006 (2016).
15. Wang, H. C. *et al*. Mesoporous silica particles integrated with all-inorganic $CsPbBr_3$ perovskite quantum-dot nanocomposites (MP-PQDs) with high stability and wide color gamut used for backlight display. *Angew. Chem. Int. Ed.* **55**, 7924–7929 (2016).
16. Pan, J. *et al*. Air-stable surface-passivated perovskite quantum dots for ultra-robust, single- and two-photon-induced amplified spontaneous emission. *J. Phys. Chem. Lett.* **6**, 5027–5033 (2015).
17. Li, J. *et al*. 50-Fold EQE improvement up to 6.27% of solution-processed all-inorganic perovskite CsPbBr3 QLEDs via surface ligand density control. *Adv. Mater.* **29**, 1603885 (2017).
18. Fu, Y. *et al*. Nanowire lasers of formamidinium lead halide perovskites and their stabilized alloys with improved stability. *Nano Lett.* **16**, 1000–1008 (2016).
19. Meyns, M. *et al*. Polymer-enhanced stability of inorganic perovskite nanocrystals and their application in color conversion LEDs. *ACS Appl. Mater. Interfaces* **8**, 19579–19586 (2016).
20. Raja, S. N. *et al*. Encapsulation of perovskite nanocrystals into macroscale polymer matrices: enhanced stability and polarization. *ACS Appl. Mater. Interfaces* **8**, 35523–35533 (2016).
21. Kamminga, M. E. *et al*. Confinement effects in low-dimensional lead iodide perovskite hybrids. *Chem. Mater.* **28**, 4554–4562 (2016).
22. Carrero, S. G., Galian, R. E. & Prieto, J. P. Organometal halide perovskites: bulk low-dimension materials and nanoparticles. *Part. Part. Syst. Charact.* **32**, 709–720 (2015).
23. Stoumpos, C. C. *et al*. Ruddlesden-popper hybrid lead iodide perovskite 2D homologous semiconductors. *Chem. Mater.* **28**, 2852–2867 (2016).
24. Saparov, B. & Mitzi, D. B. Organic-inorganic perovskites: structural versatility for functional materials design. *Chem. Rev.* **116**, 4558–4596 (2016).
25. Sum, T. C. & Mathews, N. Advancements in perovskite solar cells: photophysics behind the photovoltaics. *Energy Environ. Sci.* **7**, 2518–2534 (2014).
26. Cha, J. H. *et al*. Photoresponse of $CsPbBr_3$ and Cs_4PbBr_6 Perovskite Single Crystals. *J. Phys. Chem. Lett.* **8**, 565–570 (2017).
27. Zhang, Y. *et al*. Zero-dimensional Cs_4PbBr_6 perovskite nanocrystals. *J. Phys. Chem. Lett.* **8**, 961–965 (2017).
28. Saidaminov, M. I. *et al*. Pure Cs_4PbBr_6: highly luminescent zero-dimensional perovskite solids. *ACS Energy Lett.* **1**, 840–845 (2016).
29. Brandstater, A. *et al*. Low-dimensional chaos in a hydrodynamic system. *Phys. Rev. Lett.* **51**, 1442–1445 (1983).
30. Gu, Z. H. & Fahidy, T. Z. Visualization of flow patterns in axial flow between horizontal coaxial rotating cylinders. *Canad. J. Chem. Eng.* **63**, 14–21 (1985).

Acknowledgements

This research was supported by Basic Science Research Program through the National Research Foundation of Korea (NRF) funded by the Ministry of Education, Science and Technology" (NRF-2016R1A2B4015801). This research was also supported by Basic Science Research Program through the National Research Foundation of Korea (NRF) funded by the Ministry of Education (NRF-2017R1D1A1B03028781). This research was also supported by the National Research Foundation of Korea (NRF-2017R1A6A3A11034559). And this work was supported by the World Class 300 Project(R&D)(S2561932) of the SMBA(Korea).

Author Contributions

Y.H.S. designed and wrote this study. S.H.C. and W.K.P. contributed to discussion about Taylor flow. J.S.Y., S.B.K., B.K.K., S.R.P., and Y.S.S. performed the optical characteristics. W.S.Y., and D.H.Y. revised the manuscript and supervised the project, and all authors discussed the results and contributed this manuscript.

Additional Information

Supplementary information accompanies this paper at https://doi.org/10.1038/s41598-018-20376-3.

Competing Interests: The authors declare that they have no competing interests.

Publisher's note: Springer Nature remains neutral with regard to jurisdictional claims in published maps and institutional affiliations.